LIMNOLOGY and OCEANOGRAPHY

ASLO

Limnol. Oceanogr. 70, 2025, 3186–3201
Published 2025. This article is a U.S. Government work and is in the public domain in the USA. *Limnology and Oceanography* published by Wiley Periodicals LLC on behalf of Association for the Sciences of Limnology and Oceanography.
doi: 10.1002/lno.70173

RESEARCH ARTICLE

Broad-scale climate patterns combined with local flow and turbidity disturbances structure the seasonality of gross primary production in an aridland river

Betsy M. Summers,[1,2*] Robert O. Hall Jr.,[3] Justin K. Reale,[2,a] Eric Joseph,[1] Mark C. Stone,[1,b] David J. Van Horn[4]

[1]Department of Civil, Construction & Environmental Engineering, University of New Mexico, Albuquerque, New Mexico, USA; [2]US Army Corps of Engineers, Albuquerque, New Mexico, USA; [3]Flathead Lake Biological Station, University of Montana, Polson, Montana, USA; [4]Department of Biology, University of New Mexico, Albuquerque, New Mexico, USA

Abstract

Both local and global climate phenomena shape the hydrologic regimes of watersheds. For aridland rivers in the southwestern United States, peak flows occur during two distinct periods: spring snowmelt and summer monsoons. Although discharge (*Q*) is a primary driver of variation in the production and consumption of instream organic matter, or stream metabolism, few connection have been made regarding how climate impacts ecosystem processes through changes in flow and related disturbances. We considered how variation in disturbance variables, specifically *Q* and associated changes in turbidity, affected gross primary production during spring snowmelt and summer monsoons in the Rio Grande. Nine years of continuous environmental data (*Q*, turbidity, light) and climate indices (i.e., El Niño-Southern Oscillation and Monsoon Index) were used to explain the variation in gross primary production estimates. We found that relationships were sensitive to the timescale of disturbance: at the seasonal scale, high snowmelt *Q* decreased spring mean gross primary production, while at the daily scale, high turbidity, and to a lesser extent *Q*, reduced gross primary production during summer. Also, mean *Q* and turbidity disturbances were uncoupled in spring and inversely related in summer. We conclude that long-term datasets are essential to uncover emergent relationships between broad-scale climate patterns and ecosystem processes and are necessary to better understand how hydroclimatic variability drives ecosystem processes at varying time scales in rivers across Earth.

Interrelated global and regional climate phenomena, including those associated with sea surface temperature fluctuations (e.g., El Niño-Southern Oscillation [ENSO]), monsoon systems (e.g., North American Monsoon), and large-scale disturbances (e.g., atmospheric rivers), all influence the hydrologic regimes of streams and rivers (Dettinger and Diaz 2000; Gochis et al. 2006; Dettinger et al. 2011; Sagarika et al. 2015). For example, ENSO delivers seasonally predictable precipitation that varies according to global position and temporally with the phase of the phenomenon (Ropelewski and Halpert 1996; Stone et al. 1996). These precipitation patterns, in turn, drive characteristic changes in discharge in streams and rivers draining affected catchments (Molles Jr and Dahm 1990; Wanders and Wada 2015; Clark et al. 2014). ENSO-related variation in precipitation and discharge also affects surface water quality, including nutrient and sediment loads, and the transport of these constituents to downstream receiving water bodies (Keener et al. 2010; Acuña et al. 2005; Morera et al. 2017).

Although the effects of broad-scale climate phenomena are known for streamflow, sediment and solute transport, and

*Correspondence: shaferbetsy@gmail.com

[a]Present address: U.S. Geological Survey, Oregon Water Science Center, Portland, OR, USA

[b]Present address: Department of Biological Systems Engineering, University of Nebraska—Lincoln, Lincoln, Nebraska, USA

Associate editor: Grace Wilkinson

biogeochemical cycling, few links have been made to river metabolism. Gross primary production (GPP) and ecosystem respiration (ER) in streams and rivers are dynamic and highly variable across years, causing the balance between these two processes (carbon production vs. carbon consumption), and hence carbon availability, to vary annually (Marzolf et al. 2024; Ulseth et al. 2018; Summers et al. 2020). The dominant controls on stream metabolism are light and discharge (Bernhardt et al. 2018, 2022) and these environmental controls vary spatially across climate regions (Savoy et al. 2019) and river networks (Young and Huryn 1996; Dodds et al. 2018; Hosen et al. 2019), and temporally across seasons (Beaulieu et al. 2013). For example, high flow reduces GPP by decreasing light availability for photosynthesis as water depth and turbidity increase (Julian et al. 2008), shifting metabolism toward heterotrophy, as primary producers are more susceptible to increases in discharge than heterotrophic assemblages (Uehlinger and Naegeli 1998; Atkinson et al. 2008; O'Connor et al. 2012). However, we know less about how flow variation controls metabolism across and within years as a function of broad-scale climate patterns. This uncertainty in relationships that span varying temporal scales (e.g., hours to years) risks misunderstanding the drivers of GPP in absence of multi-year time-series data.

The impacts of broad-scale climate drivers on stream metabolic processes are particularly relevant in regions where climate patterns strongly control precipitation and subsequent stream flow. In the southwestern United States, hydrologic variation occurs seasonally, with periods of high discharge in spring from snowmelt and in summer from short-lived and spatially discrete monsoon rainstorms. Winter precipitation as snow in high-elevation headwaters is linked to ENSO, with elevated snowfall in El Niño years causing increased spring runoff. Drivers of the North American Monsoon pattern are complex, with seasonal shifts related to variation in land and sea surface temperatures (Grantz et al. 2007) and extreme events linked to moisture surges from the Gulf of California and the occurrence of convective and frontal systems (Duan et al. 2024). Although both climate phenomena affect precipitation in this region, hydrologic conditions differ between seasons. Snowmelt discharge originates in high-elevation portions of the watershed that are highly vegetated and minimally erosive, and thus associated increases in turbidity are due to mobilization of in-channel sediments (Nordin and Beverage 1965). In contrast, monsoon events occur throughout the watershed, including in lower elevation portions with minimal vegetation and highly erosive geology (Wilcox et al. 2003), dramatically increasing turbidity as soils are moved from the landscape into stream channels. Interestingly, during summer, turbidity can greatly increase in perennial stream reaches with only minimal increases in discharge when low-volume, but sediment-rich inputs occur from small intermittent tributaries (Fig. 1). Additionally, the temporal scale of these disturbances differs, with (sub)monthly-scale changes in discharge and turbidity associated with snowmelt, whereas monsoons produce (sub)daily-scale impacts (Fig. 1).

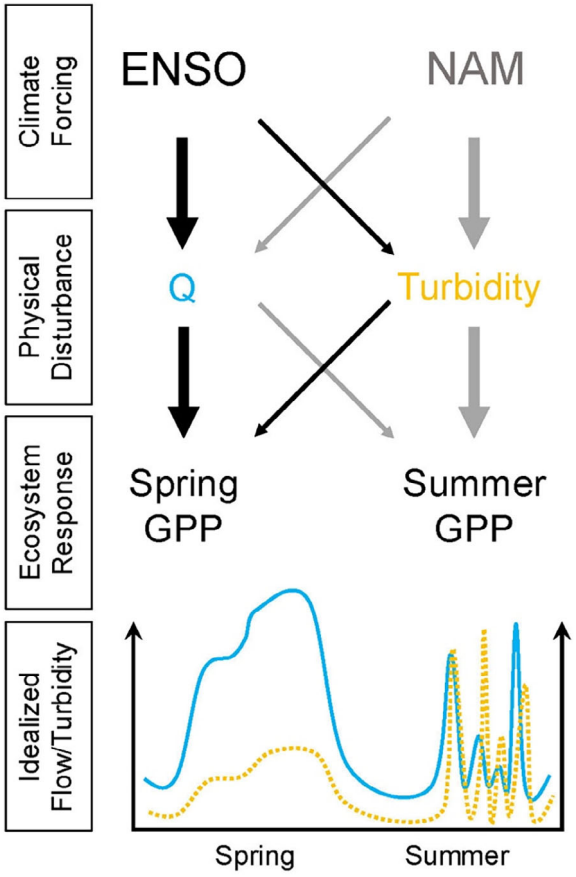

Fig. 1. Hypothesized linkages between climate (El Niño-Southern Oscillation—ENSO [black arrows] and the North American Monsoon—NAM [gray arrows]), physical disturbances (discharge [blue] and turbidity [tan]), and ecosystem response (gross primary production—GPP) during dynamic seasonal periods, spring snowmelt and summer monsoons. Conceptual graph shows idealized flow and turbidity disturbance patterns. Each arrow represents a testable relationship between predictor and response variables. Thick arrows are hypothesized to have stronger effects between predictor and response variables compared to thin arrows.

In this study, we use long-term continuous dissolved oxygen (DO) and water quality data to assess how two types of disturbance that are influenced by broad-scale climate phenomena, discharge and turbidity events, affect variation in primary production in a large aridland river during two hydrologically distinct periods, spring snowmelt (March–June), and summer monsoons (July–September) (Fig. 1). We developed an a priori data analysis plan that we conducted at two time scales, seasonal and daily means, to match the scales of the analyses to the disturbances. We hypothesized that a coarser temporal scale (seasonal mean) would be most appropriate for long-duration disturbances (i.e., spring snowmelt) whereas a finer temporal scale (daily mean) would best identify short-duration disturbance (i.e., discrete summer rainfall-runoff)

impacts on GPP. Additionally, climate patterns were structured differently in statistical models based on the time scale of analysis to understand the role of complex climate-disturbance-ecosystem linkages. We predicted that in the spring, ENSO affects seasonal discharge, and to a lesser extent turbidity, such that El Niño conditions (increased snowpack, discharge, and turbidity) reduce GPP, while La Niña conditions (decreased snowpack, discharge, and turbidity) enhance GPP. We predicted that North American Monsoon precipitation events in the summertime would affect short-duration increases in turbidity that are often associated with minimal increases in daily mean discharge, lowering rates of GPP during wetter monsoon years.

Methods

Study site

The Rio Grande is the fifth longest river in the United States, flowing 2830 km across three states. The Middle Rio Grande is defined as the reach extending from the Otowi streamflow gauge (US Geological Survey, USGS #08313000) above Cochiti Reservoir to Elephant Butte Reservoir in New Mexico (Fig. 2). Within the Middle Rio Grande, snowpack from high-altitude sub-basins contributes to spring runoff, while monsoonal rainstorms control variation in baseflow summer discharge. Most rainfall occurs during the North American Monsoon Season in July and August, based on point precipitation frequency estimates (NOAA Atlas 14; https://hdsc.nws.noaa.gov/hdsc/pfds/) and is highly variable in space and time. During periods of elevated discharge derived from snowmelt or rainfall runoff, intermittent streams contribute flows and transport sediments to the Middle Rio Grande (Ortiz 2004; Swanson et al. 2011).

Our study site located in Bernalillo, New Mexico at the US 550 Highway Bridge ("Bernalillo"; 35°19′19.53″N, 106°33′26.87″W) is in a transitional zone for river geomorphology and land use (Fig. 2). Upstream of this site, the riverbed is armored with coarse substrate. At the study site, the substrate is a mixture of coarse gravel and sand throughout the low sloped channel, ~ 0.001 m m^{-1} (Massong et al. 2010) and changes downstream to sand riverbed. This site is also at a land use transition point from a predominately grassland, riparian forest, and shrub/scrub land-cover upstream to an urban development land use downstream of the site (Regier et al. 2020).

The Middle Rio Grande region has undergone considerable geomorphic changes due to the engineering of the channel and construction of Cochiti Dam in 1973, which is located ~ 45 km upstream of this study site and is operated for flood and sediment control. Specific changes to the Middle Rio Grande at Bernalillo include increased river depth and decreased width (degradation) due to changes in sediment loads downstream of Cochiti Dam (Davis et al. 2014). Channel incision and high riverbanks prevent overbanking (Massong et al. 2006) and the river is constrained in a single main channel while historic minor flow paths are mostly abandoned.

Data sources

We combined high temporal resolution data for water quality, meteorological, and hydrological variables to model metabolism parameters (GPP, ER, and gas exchange [K]). We used 9 yr of daily metabolism estimates to explore relationships between GPP and physicochemical variables at different time scales.

Physicochemistry

A long-term water quality record from 2007 to 2019 provided high resolution (15-min intervals) time series of DO (mg L^{-1}), water temperature (°C), turbidity (NTU), specific conductance (μS cm^{-1}), and pH. Data were collected with Yellow Springs Instruments (YSI); YSI 6920 and YSI 6920 V2 instruments were used from 2007 to 2012, and YSI EXO instruments were used from 2013 to 2019. A difference in these sensor models is the improvement in maximum detection limit in turbidity from 1200 NTU to > 4000 NTU, so we capped the maximum value at 1200 NTU to compare turbidity measurements across years. Instruments were serviced every 2–4 weeks following USGS standard operating procedures (Wagner et al. 2007). Time gaps in the water quality record were due to burial of the probe or instrument, biofouling, malfunctioning of the probe, or temporary removal of the sensor from the site (e.g., data from 2009 are absent). When possible, time gaps were filled using data collected by the United States Geological Survey (USGS gauge #08329400) and Albuquerque Metropolitan Arroyo Flood Control Authority. Data quality was assessed for the entire record using Aquarius Workstation 3.10 (Aquatic Informatics) and corrected for drift and fouling with the spline interpolation function when applicable.

Hydrology and river depth

Discharge data were collected at 15-min intervals at stream gages maintained by the USGS (Nos. 08317400, 08317950, 08319000, 08328950, 08329835, 08329918). We used water quality parameters to calculate a mean travel time from Bernalillo to USGS gage 08329918 (Rio Grande at Alameda Bridge) of 5 h. We then estimated discharge at Bernalillo based on the time corrected discharge at USGS gage 08329918 by removing intermittent flows measured between the two locations based on USGS gage 08329900 (North Floodway Channel near Alameda). The remaining USGS gages were used as hydrographic comparisons to further distinguish between flows at USGS gage 08329918 which originated above and below Bernalillo. Field measurements of channel width, area, velocity, and discharge taken by the USGS that spanned the study period (2007–2019) were used to develop power law functions to estimate mean river depth from the continuous

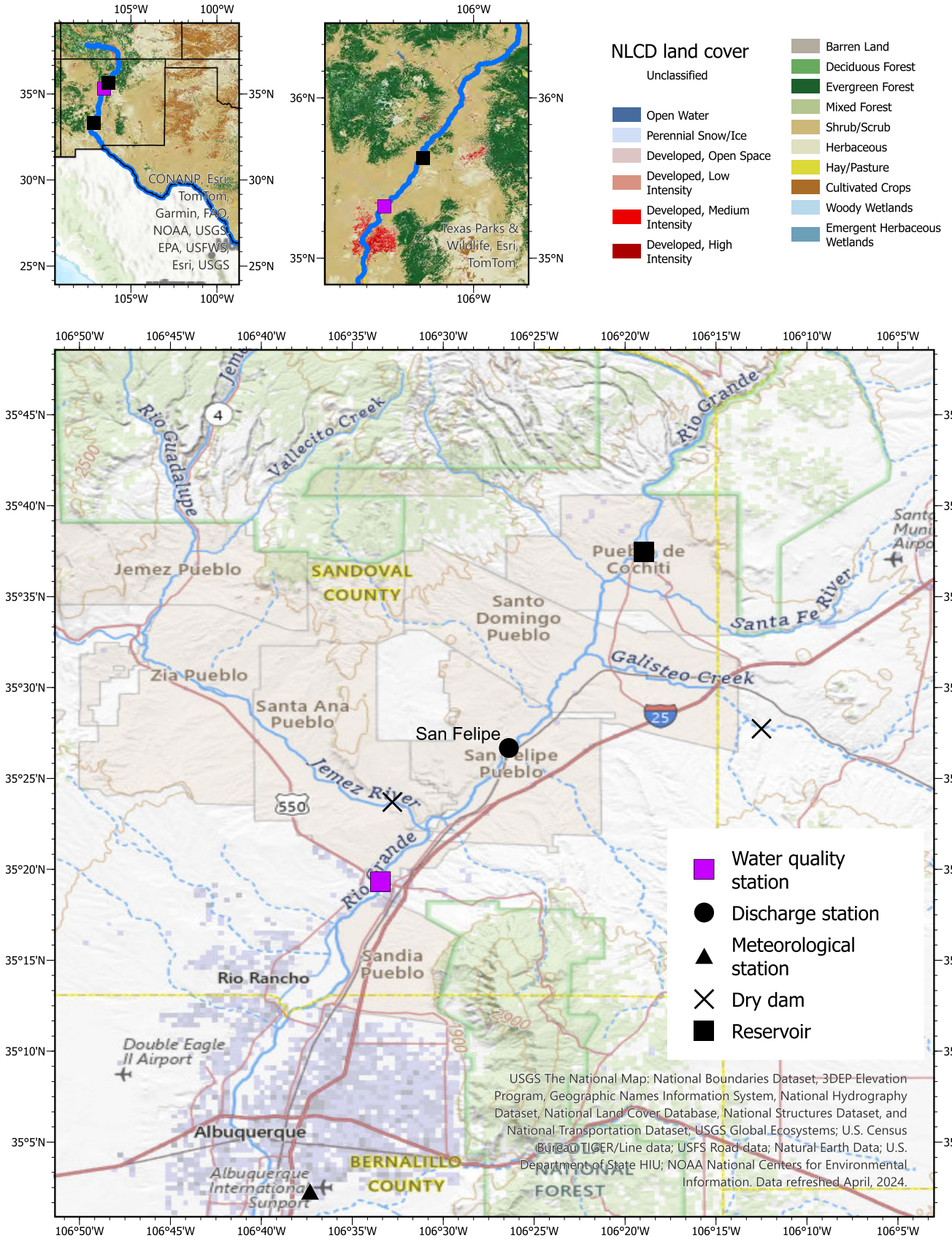

(Figure legend continues on next page.)

discharge record (Leopold et al. 1953). The river channel was assumed to be rectangular.

Meteorology

Air pressure and shortwave radiation were obtained from the National Aeronautics and Space Administration's (NASA) North American Land Data Assimilation System (NLDAS) as gridded datasets at 1-h intervals and 0.125° spatial resolution. Shortwave radiation (I) was converted to photosynthetic active radiation (PAR [μmol m^{-2} s^{-1}]) following Meek et al. (1984); $PAR = I \times 2.04$. The daily light integral (μmol m^{-2} d^{-1}) was calculated from instantaneous measurements of PAR. We accessed the MesoWest data portal (https://mesowest.utah.edu) for barometric pressure (mb) collected in hourly to 5-min intervals at the KABQ station (35°2′30.01″N, 106°36′52.99″W). Barometric pressure was corrected for elevation differences between meteorological and water quality sites. Meteorological data were interpolated by applying a cubic spline function from the *zoo* package (Zeileis and Grothendieck 2005) in R (2018, R Core Team, Vienna, Austria) to match the 15-min interval of water quality data.

Climate

Historical climate information on the ENSO phenomenon was taken from the National Oceanic and Atmospheric Association (https://origin.cpc.ncep.noaa.gov). We used the Oceanic Niño Index (ONI) value that references the 3-month running mean of sea surface temperature anomalies for the December–February period as a continuous variable. Typically, ENSO categories—El Niño (EN), La Niña (LN), Medial (M)—are identified from this ONI and are used to represent precipitation and subsequent flow conditions, which occur as snowpack and snowmelt discharge in the southwestern US region (Molles Jr and Dahm 1990; Summers et al. 2020). During this study, a combination of EN (2007, 2010, 2015–2016, 2019; $n = 5$), LN (2008, 2011–2012, 2018; $n = 4$), and M (2013–2014, 2017; $n = 3$) conditions occurred from 2007 to 2019, excluding the year 2009. We used the ONI as a continuous variable of ENSO condition with positive and negative values for ONI representing varying EN (wet) and LN (dry) conditions, respectively, based on deviations from the ONI zero defined by the centered 30-yr period that is updated every 5 yr. Note that a couple of years had the same ONI values, specifically years 2013 and 2014 (ONI = −0.4) and 2012 and 2018 (ONI = −0.9); there were seven unique ONI values during this study (Fig. 3).

We developed a site-specific Monsoon Index using monthly mean PRISM precipitation data (https://cran.r-project.org/web/packages/prism/vignettes/prism.html) from June through September for each year (2009–2018) relative to the drainage area above the study site but downstream from Cochiti Dam, to capture the high spatial heterogeneity in rainfall (Gutzler 2004). The approximate drainage area impacting the study site was cropped using the USGS Hydrologic Unit Codes as guidance for extracting PRISM precipitation data with a 4-km grid resolution using the prism package (Edmund et al. 2025) in R. Monthly mean precipitation data were summed across the summer season for each year and compared to a 30-yr mean to generate anomalies that represented interannual variation with positive and negative values for the Monsoon Index representing wet and dry conditions, respectively. A total of nine Monsoon Index values were unique (i.e., one for each year) for this study (Fig. 3).

Metabolism estimation

We estimated reach-scale metabolism using *streamMetabolizer* (version 0.11.3) which allows for gross primary production (GPP), ER, and gas exchange between air-water to be free parameters in the DO model (Odum 1956; Appling et al. 2018). The DO model, Eq. 4, was implemented to estimate metabolism at each timestep:

$$\Delta O_{mod,i,d} = \left(\frac{GPP_d}{z_{i,d}} \times \frac{PPFD_{i,d}}{\overline{PPFD_d}}\right) + \left[\left(\frac{ER_d}{z_{i,d}}\right) + f_{i,d}(K600_d)\left(O_{sati,d} - O_{mod,i,d}\right)\right] \times \Delta t \quad (1)$$

where the change in modeled oxygen concentration (ΔO_{mod} [mg L^{-1}]) at i (15-min timestep interval) for a day (d) is a function of daily average rate of gross primary production (GPP [gO_2 m^{-2} d^{-1}]), observed photosynthetic photon flux density (PPFD), and daily mean of PPFD (PPFD); the daily average rate of ER (gO_2 m^{-2} d^{-1}) and GPP; estimated mean river depth (z [m]); and K600 is the gas exchange rate coefficient scaled for temperature using a Schmidt number of 600 and converted to an oxygen specific gas exchange rate through the function (f) (Jähne et al. 1987) and driven by the difference of theoretical saturation (O_{sat} [mg L^{-1}]) and modeled (O_{mod} [mg L^{-1}]) oxygen concentrations (Appling et al. 2018). In this state-space model, O_{mod} represents the unobserved state of oxygen concentration.

Continuous data were prepared into two overlapping time period batches for *streamMetabolizer* and run on a high performance computer. We implemented a Bayesian model variant with identical partial pooling of K600 across days for both batches, then compared K estimates for across years (Supporting Information Fig. S1). For each batch run, a piecewise relationship, consisting of seven linearly connected points, was used to relate K600 values to daily mean Q (Appling et al. 2018) with the relationship bounded by the minimum and maximum Q values.

(Figure legend continued from previous page.)

Fig. 2. Study site (Bernalillo) located on the Middle Rio Grande noted by a water quality sensor (pink square), along with meteorological stations (triangle), and US Geological Survey gauge for discharge (circle). Water quality station is 45 km from Cochiti Dam. National Land Cover Dataset (NLCD) is shown for 2016. Meteorological stations SolRad and Kabq are separate stations but overlap due to the spatial scale.

Default and previous estimates of metabolism in the Middle Rio Grande from Summers (2019) and (Lusk et al. 2012) were used to inform priors of mean (3.1 and − 3.1 g O_2 m^{-2} d^{-1}) and standard deviation (3.1 and 7.1 g O_2 m^{-2} d^{-1}) values of GPP and ER, respectively. Additionally, we used a mean center for K600 of 9.4 d^{-1}, a log-normal distribution with a standard deviation of 0.7, and a sigma of 0.05 based on methods identified by Ulseth et al. (2019). Markov chain Monte Carlo simulations were run with 1000 burn-in steps and 500 saved steps, similar to (Arroita et al. 2019) and (Appling et al. 2018). We used the following criteria for selecting reasonable model estimates of GPP: (1) the Gelman-Rubin $R < 1.1$ (Gelman et al. 1996) to indicate convergence of Markov chain Monte Carlo simulations for each parameter (GPP, ER, and K); (2) comparison of subdaily observed and modeled DO concentrations to validate goodness of fit (i.e., timing and concentrations values); and (3) identifying unrealistic estimates where the mean daily value exceeded 1.96 times the daily standard deviation in the negative and positive direction for GPP and ER, respectively. We excluded days from the data analyses if the model selection criteria were violated. Instances when GPP was < 0 but > -0.5 were rounded to 0.1 because these days still represent reasonable, albeit low, biological activity (Appling et al. 2018). We checked for covariance in GPP and ER with K estimates (Supporting Information Fig. S2), which could indicate equifinality in parameter estimates. Although post-processing steps included both GPP and ER model output, our paper solely focuses on GPP. Daily estimates of GPP, *Q*, PAR, and water quality variables (Supporting Information Fig. S3) are available at the Environmental Data Initiative data repository (Van Horn and Summers 2025).

Data analysis

We selected 9 yr (2010–2018) from the larger GPP dataset to test for relationships between climate indices, disturbance variables, and GPP during two hydrologically distinct seasonal periods (Fig. 1). These 9 yr were more complete (> 80% of daily GPP estimates available for two consecutive months in spring and summer seasons) than the first 3 yr (2007–2009) of data, which contained substantial gaps and were thus excluded from the analyses. Seasonal periods were designated as spring snowmelt (March 1–June 30) and summer monsoon (July 1–September 30) based on known seasonal and annual variation in hydrologic patterns. To understand the effects of climate on interannual variation in physical drivers and ecosystem processes, we framed these testable connections between climate index—watershed condition—ecosystem process in Fig. 1 at two time scales (seasonal and daily means) and we organize our results into two distinct seasonal periods, spring and summer, that vary in disturbance time scale.

Seasonal scale analysis

We regressed seasonal mean *Q*, turbidity, and GPP with two climate indices—the Oceanic Niño Index as a continuous variable of ENSO condition and our developed relative Monsoon Index—for the snowmelt and monsoon time periods. We also used simple linear regression models to test relationships between seasonal mean GPP and physical drivers (*Q*, turbidity) during the spring snowmelt and the summer monsoon periods—variables were log transformed. We report the strength and uncertainty in these relationships using predictor variable coefficients, including slope, 95% confidence intervals (CIs), and (r^2).

Daily scale analysis

We investigated the functional response in daily GPP to multiple environmental predictors (*Q*, turbidity, and PAR) during spring and summer periods using hierarchical generalized additive models (HGAMs) with the *mgcv* package version 1.8-34 (Wood 2011). The HGAMs provide flexibility in

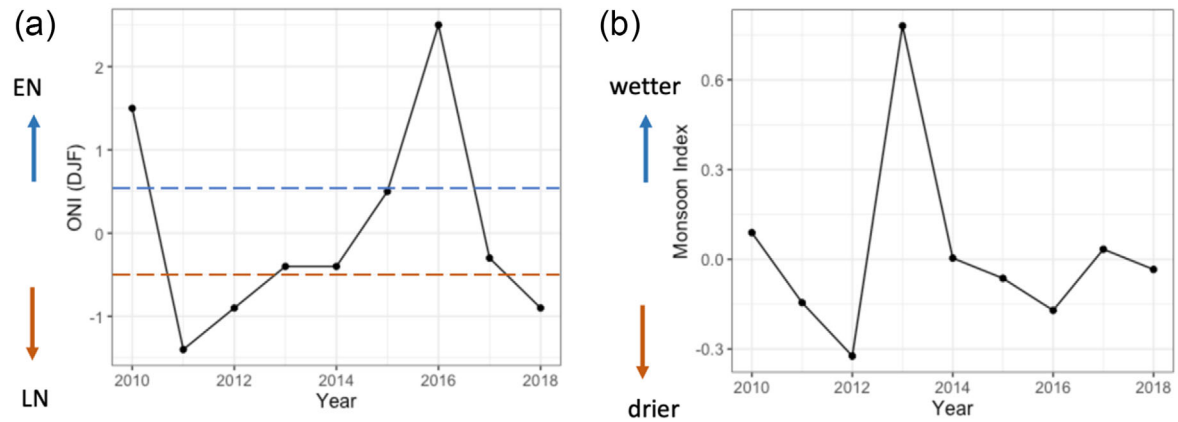

Fig. 3. (**a**) Oceanic Niño Index (ONI) and (**b**) Monsoon Index for the study period. The ONI value represents the 3-month running mean of sea surface temperature anomalies for the December–February (DJF) period. The ONI zero value is based on a centered 30-yr base period updated every 5 yr. El Niño or La Niña conditions occur when ONI is ± 0.5, respectively, as indicated by dashed blue and red lines, respectively. The Monsoon Index represents regional conditions from the contributing watershed for summer precipitation. The Monsoon Index zero value is based on a 30-yr mean, and deviation indicates relative wetter (positive values) or drier (negative values) conditions.

capturing nonlinear relationships in environmental data, allow for predictor variables to be additive, and account for structured data that is nested in multiple levels by grouping data (Wood 2017; Pedersen et al. 2019). Following our conceptual figure (Fig. 1), we first used HGAMs to test for the effects of climate index (ONI, Monsoon Index) as a grouping variable for predictor variables in explaining the response variable. Although climate indices are inherently continuous values with respect to long-term mean, we treated these as groups or as a categorical factor to account for potential repeatable values (i.e., repeatable ONI values). We compared model structures of HGAMs by varying the influence of a common or "global" smoothing parameter and "wiggliness" or change in functional response of the smoother for the predictors (Pedersen et al. 2019), and whether the climate variable influenced the model structure (Table 1). We started with a simple model structure that included global smoothing functions of predictors (log *Q*, log turbidity, and PAR) in predicting the response of (log) GPP. Then, we added structure to the model by incorporating climate index (ONI for spring and Monsoon Index for summer) as a random intercept or grouping variable (or both) to explain the change in functional response relative to the global trend. We selected the HGAM that produced the lowest Akaike Information Criterion (Akaike 1979) in explaining daily GPP for each seasonal period (*see* Supporting Information 1 for model testing). This final model was the HGAM model structure that accounted for random intercept and intergroup variation from the global smoother and differing change in functional response across climate groups but had a similar function response shape. In summary, the "best" model structure included ONI or Monsoon Index as a random effect and allowed for varying coefficients. Each HGAM structure included the restricted maximum likelihood method to predict the smoothing variable (i.e., lambda) that fits the data with a Gaussian distribution (Wood 2001). We assessed model residuals for normality and random effects for appropriateness using quantile plots. The HGAM outputs were visualized using the *gratia* (Simpson and Singmann 2021) and *visreg* packages (Breheny et al. 2020). After selecting the HGAM structure, we assessed the effects of global smoothers on daily GPP based on deviation from the zero *y*-axis. Similarly, we assessed the effect of climate (ONI, Monsoon Index) on intergroup variation in the response of daily GPP to predictors by examining the deviation of the CI from the zero *y*-axis from each group, which represents the departure from the global smoother trend. We also included a *p*-value in the model output where $p < 0.05$ provides evidence that a group varies from the global trend (Supporting Information 1). For example, when the functional response (effect) becomes negative, this indicates lower GPP at higher *Q* compared to the global trend, whereas convergence toward the zero *y*-axis means a similar response shape (coefficient) to the global but differs by intercept (Pedersen et al. 2019).

Results

Springtime linkages (ENSO–snowmelt–GPP)

Seasonal scale analysis—High snowmelt Q decreased GPP

During snowmelt, mean discharge varied greatly, ranging from 16.3 $m^3 s^{-1}$ in a La Niña year (2018) to 82.6 $m^3 s^{-1}$ (2017—M). Spring mean log *Q* tended to be higher when ONI was positive (i.e., EN category) with a 24% increase in *Q* per unit increase in ONI (slope = 0.24, CI = −0.08, 0.56, $r^2 = 0.21$) but this relationship was stronger when a pronounced outlier, 2017 (M), was removed (slope = 0.27, CI = 0.08, 0.45, $r^2 = 0.61$). This year followed a sequence of two higher snowmelt and average monsoon years (Fig. 4; Supporting Information Fig. S4). Spring mean turbidity was relatively low (< 200 NTU) for most years, except for 2012 when mean turbidity (390 NTU) was nearly twofold higher, likely attributed to wildfire effects (Dahm et al. 2015; Reale et al. 2015), resulting in no clear relationship between annual mean log turbidity and mean log *Q* (slope = 0.32, CI = −0.83, 1.46, $r^2 = 0.0$) (Fig. 4). ONI had little explanatory power over spring mean log turbidity (slope = 0.04, CI = −0.46, 0.55, $r^2 = 0.0$).

During the snowmelt period, spring mean (log) GPP declined with mean log *Q* (slope = −1.01, CI = −1.7, −0.3, $r^2 = 0.59$), with a 101% decrease in GPP values associated with a 100% increase in *Q* (Fig. 4). A few years of high spring mean GPP corresponded with lower spring mean log turbidity (2018, 2011, and 2013), although the turbidity effect on GPP was uncertain due to a highly influential year (2012) (slope = −0.42, CI = −1.2, 0.4, $r^2 = 0.08$). The effect was larger (~ 100% decrease in GPP) but still uncertain (CI = −2.2, 0.3, $r^2 = 0.28$) when 2012 was removed. When linking climate patterns and ecosystem processes, spring mean rates of GPP were higher when ONI values were negative (i.e., LN category, low snowmelt *Q*) (slope = −0.29, CI = −0.70, 0.11, $r^2 = 0.19$) with a stronger relationship when 2017 was removed (slope = −0.32, CI = −0.64, −0.01, $r^2 = 0.43$) (Fig. 4; Supporting Information Fig. S4), indicating that high snowmelt years lower spring mean GPP. Overall, mean GPP was highest in 2018 (2.4 g O_2 m^{-2} d^{-1}; LN) and 2011 (2.3 g O_2 m^{-2} d^{-1}; LN) while in other years (2014–2017) mean GPP was generally low (GPP < 1.0 g O_2 m^{-2} d^{-1}) during the spring snowmelt period.

Daily scale analysis—ONI grouping explains the effects of Q *on GPP in Springtime*

Global trends for *Q*, turbidity, light, and ONI were influential in explaining daily GPP (CI did not include 0); both elevated *Q* and turbidity lowered GPP while light increased GPP (Fig. 5). However, *Q* had a more negative effect on GPP at $Q > 40$ $m^3 s^{-1}$ than turbidity. The influence of ONI indicated that inter-group variation in the rate of response of GPP to *Q* differed from the global response behavior for six of the seven ONI groups (ONI = −1.4, −0.9, −0.4, −0.3, 0.5, 2.5) (Fig. 5). We confirmed through testing HGAM structures that the inclusion of ONI as a grouping variable, which includes

ONI as a random effect (i.e., intercept and slope), best explained relationships between daily GPP and Q (Table 1, Supporting Information I). This finding supports our hypothesis that climate is linked with disturbance (i.e., Q) and GPP. However, inter-group variation in light and turbidity contributed less to the response in GPP given the lesser extent of climate group explaining the effect of light (two of seven ONI groups) and turbidity (three of seven ONI groups) on GPP (Fig. 5). This finding indicates the global response in GPP to turbidity and PAR was generally consistent across ENSO conditions, as seen in the response that overlaps with the zero *y*-axis (Fig. 5e, f).

Summertime linkages (monsoon–turbidity–GPP)

Seasonal scale analysis—The effect of monsoon and turbidity on GPP was uncertain

During the monsoon period, summer mean turbidity increased dramatically, ranging from 131 NTU (2016) to 505 NTU (2013) due to multiple monsoonal rainstorms even though summer mean Q was always low (range: 13.5–24.9 $m^3 s^{-1}$). However, summer mean log turbidity was variable when compared to the Monsoon Index, with one extremely wet year in 2013 (MI = 0.78) (slope = 0.56, CI = −0.77, 1.89, $r^2 = 0.001$) (Fig. 6). Interestingly, the year with the highest mean turbidity (2013) had the lowest mean Q, with mean log turbidity being inversely related to mean log Q during the monsoon period (slope = −1.75, CI = −3.06, −0.44, $r^2 = 0.53$). Summer log Q was not explained by Monsoon Index (slope = −0.16, CI = −0.77, 0.44, $r^2 = 0.0$).

During the monsoon period, summer mean log GPP was not clearly related to mean log turbidity (slope = −0.52, CI = −1.78, 8.51, $r^2 = 0.09$) as there was considerable variability in GPP at lower turbidity. Additionally, mean log GPP did not covary with either the Monsoon Index (slope = −1.11, CI = −2.34, 0.42, $r^2 = 0.18$) or the log Q (slope = −0.32, CI = −5.27, 7.98, $r^2 = 0.0$). Overall, summer mean GPP was greater than 2.0 g O_2 m^{-2} d^{-1} in multiple years (2016, 2011, and 2017) and lowest in 2014 (0.6 g O_2 m^{-2} d^{-1}).

Daily scale analysis—Monsoon grouping explains the effect of turbidity on daily GPP in summertime

Global trends for turbidity, Q, and Monsoon Index were influential in explaining daily GPP. Turbidity had a negative effect on GPP, especially when turbidity was greater than ~200 NTU (Fig. 7), which we attribute to decreased light availability required for photosynthesis. Discharge also had a negative effect on GPP, although not as strong as turbidity; the effect of Q on GPP included large uncertainty at higher Qs because Q typically did not exceed ~40 $m^3 s^{-1}$ (Fig. 7e). The positive effect of light on GPP was stronger in spring compared to summer (Figs. 5, 7) given that PAR was not significant for the global trend in summer.

The Monsoon group explained the effect of turbidity on daily GPP, with four of nine Monsoon groups differing from the global response of GPP to turbidity (MI = −0.063, = −0.145, −0.171, 0.34; Fig. 7e). Interestingly, the effect of Q on GPP for five out of nine Monsoon groupings also differed from the global trend (Fig. 7d). Again, we confirmed through testing HGAM structures that the inclusion of Monsoon as a grouping variable best explained relationships between daily GPP and turbidity (Table 1; Supporting Information II). This finding supports our hypothesis that climate is linked with disturbance (i.e., turbidity as well as Q) and GPP (Fig. 7d, e).

Table 1. Testing of hierarchical generalized additive model structure to identify best fit based on Akaike Information Criterion (AIC). Response variable is log gross primary production (GPP); predictors are log transformed discharge (log Q) and turbidity (log turbidity), and photosynthetic active radiation (PAR), with observations at the daily scale. Grouping variable is climate indices (Oceanic Nino Index [ONI] and Monsoon Index [MI] for spring and summer periods, respectively). Model type follows a similar convention as Pedersen et al. (2019) with "G" indicating global smoother functions.

			AIC	
Model type	**Structure**	**Hypothesis**	**Spring**	**Summer**
G	Global smoothers for predictors (Q, Turb, PAR)	A single, common functional response in GPP for each predictor	2712	2109
G.ONI or G.MI	Global smoothers for predictors + random intercept for climate group	G + random intercept for climate group	1781	1353
GS.ONI or GS.MI	Global smoother for predictors + random intercept for group + group-level smoothers with same coefficients	G + intergroup variation has the same wiggliness	1569	1237
GI.ONI or GI.MI	Global smoother for predictors + random intercept for group + group-level smoothers with different coefficients	G + intergroup variation has different wiggliness	1548	1201

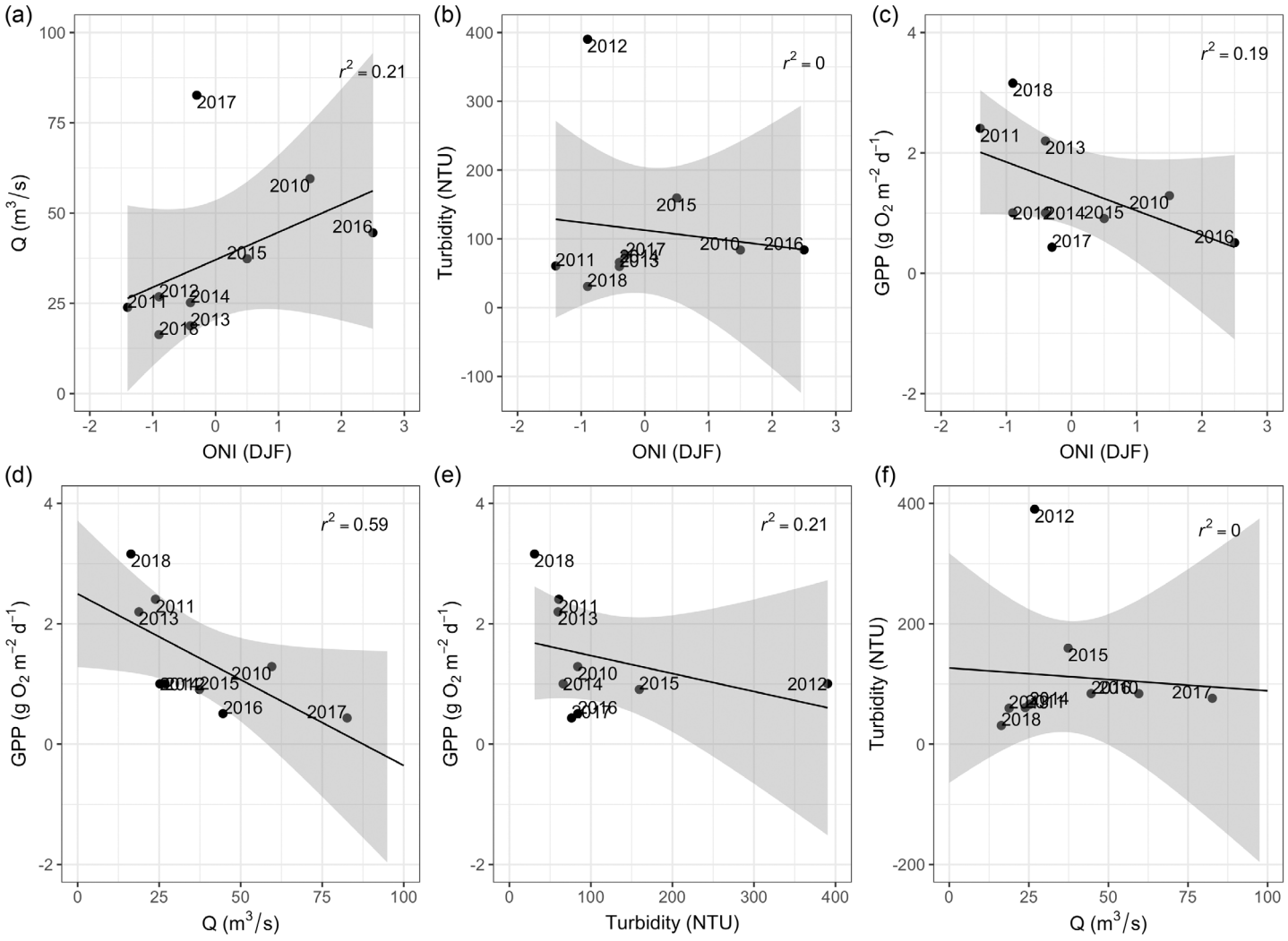

Fig. 4. Mean discharge (Q), turbidity, gross primary production (GPP), and Oceanic Niño Index (ONI) during spring snowmelt (March to June). Linear relationships were found between log GPP and log Q (slope = −1.01, CI = −1.7, −0.3, $r^2 = 0.59$). GPP, Q, and turbidity are log transformed; the axes also have a transformation but are reported as untransformed values to ease interpretation of values. [Correction added on 25 November 2025, after first online publication: Figure 4 has been updated to the correct version because the figure was mistakenly provided from the Supporting Information for Figure 4 and used in the article's initial online publication.]

Discussion

Primary productivity in the Middle Rio Grande was dynamic and highly variable across years depending on climatic, watershed, and local environmental conditions, which are commonly linked phenomena. We identify time periods of high interannual variation in GPP that coincide with spring snowmelt discharge and summer monsoons and that varying magnitudes of disturbances at the seasonal and/or daily time scale are associated with substantial within and across-year differences in GPP estimates. This study provides some evidence for linkages between instream carbon production and global climate phenomenon, suggesting that hydroclimatic variables can covary with interannual variation in metabolism (Young and Huryn 1996; Summers et al. 2020). However, this work also reveals the complexity of these patterns due to factors such as the impact of a series of wet or dry years, highlighting the need for long-term metabolism estimates to better understand climate effects on instream carbon dynamics.

Spring snowmelt controls on GPP

Snowmelt discharge in this river reach affected both annual and daily mean GPP in spring, with high snowmelt years typically associated with EN conditions reducing spring GPP. The impact of snowmelt discharge on spring GPP is strong in montane, open-canopy rivers (Ulseth et al. 2018; Summers et al. 2020; Canadell et al. 2021). This work extends these findings to large, lower elevation river systems, highlighting the importance of broad-scale hydroclimate variables in determining instream carbon production at the seasonal time scale; however, the impacts and underlying mechanisms vary between contexts.

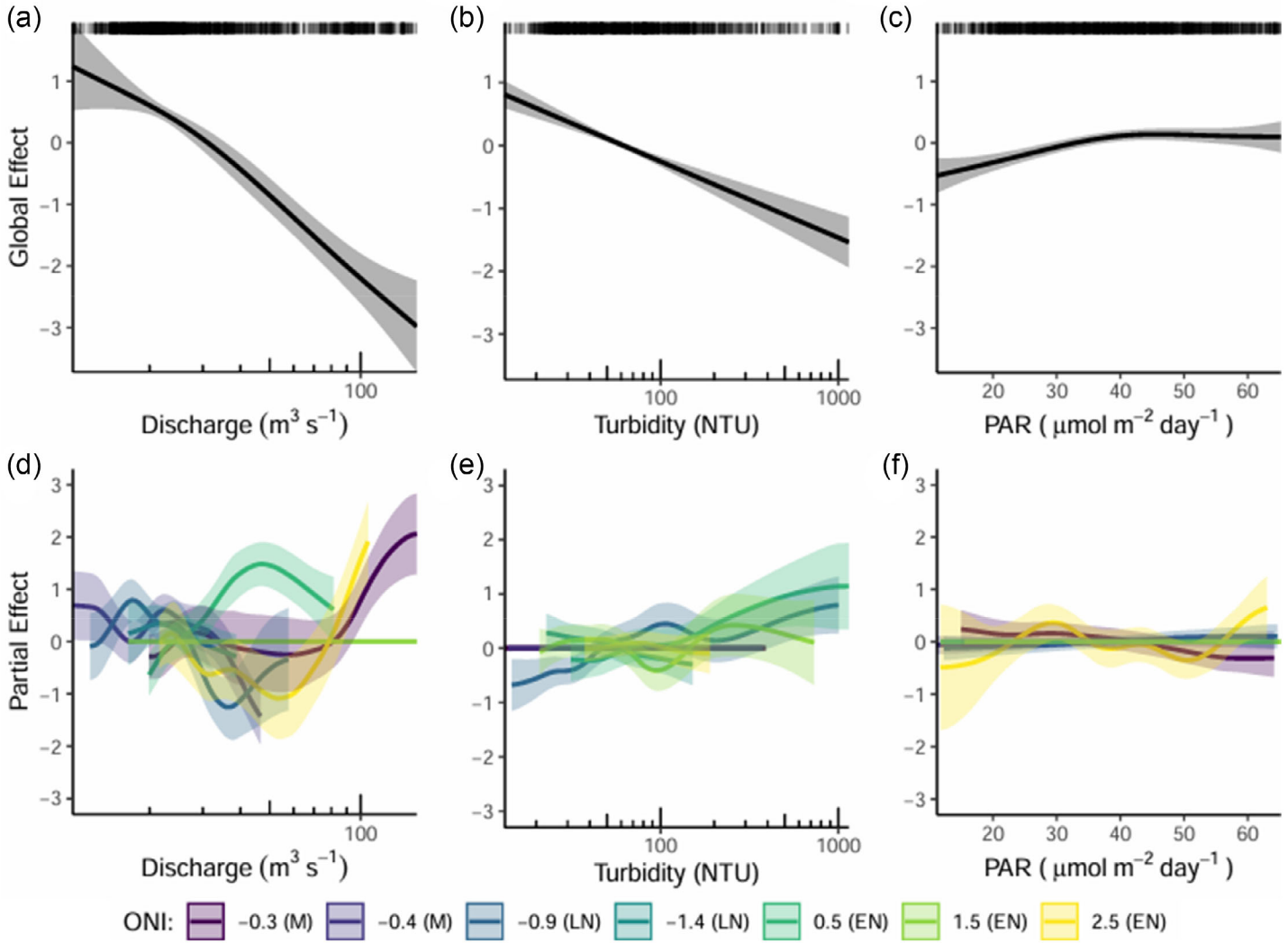

Fig. 5. Global smoother effects (**a**) discharge ($m^3\ s^{-1}$), (**b**) turbidity (NTU), and (**c**) photosynthetic active radiation (PAR, μmol $m^{-2}\ d^{-1}$) on daily GPP in spring. Group level variation in the effect of (**d**) discharge, (**e**) turbidity, and (**f**) PAR on daily GPP with Ocean Niño Index as the grouping variable. The effect on GPP varies from the global smoother when the response deviates from the zero *y*-axis. Legend shows ONI groups and categories (El Niño [EN], La Niña [LN], and medial [M]). Discharge, turbidity, and GPP are log transformed. Upper ribbon in (**a**–**c**) represents data for predictors and all plots have a 95% CI band around the smoothing trendline.

Hydrologic pulses induced by snowmelt can enhance spring GPP at the daily and seasonal scales in smaller high-elevation streams (Ulseth et al. 2018; Summers et al. 2020), likely from delivery of nutrients to instream primary producers (Sebestyen et al. 2008; Pellerin et al. 2012). In contrast, in the Rio Grande, elevated discharge from snowmelt likely physically disturbs highly mobile substrate (Uehlinger 2006) or attenuates light at the riverbed (Kirk et al. 2021), which limits GPP (Young and Huryn 1996). Thus, the reduction in mean GPP during high snowmelt years suggests that the impacts of high flows are a predictable seasonal driver of instream carbon production. Although the relationship between seasonal mean *Q* and global-scale ENSO climate events in this study was uncertain, other findings in the southwestern US show that snowpack and snowmelt are largely linked to ENSO patterns (Molles and Dahm 1990). Causes of uncertainty in predicting snowmelt hydrology based on climate conditions are likely attributed to antecedent conditions within the catchment, such as soil moisture and snow water equivalent (McNamara et al. 2005). Sequences in climate patterns may also control snowpack and snowmelt dynamics through antecedent conditions mentioned above. Specifically, in this study, snowpack during two sequential EN years (2015 and 2016) likely caused high soil moisture conditions within the watershed leading into a weak LN year with

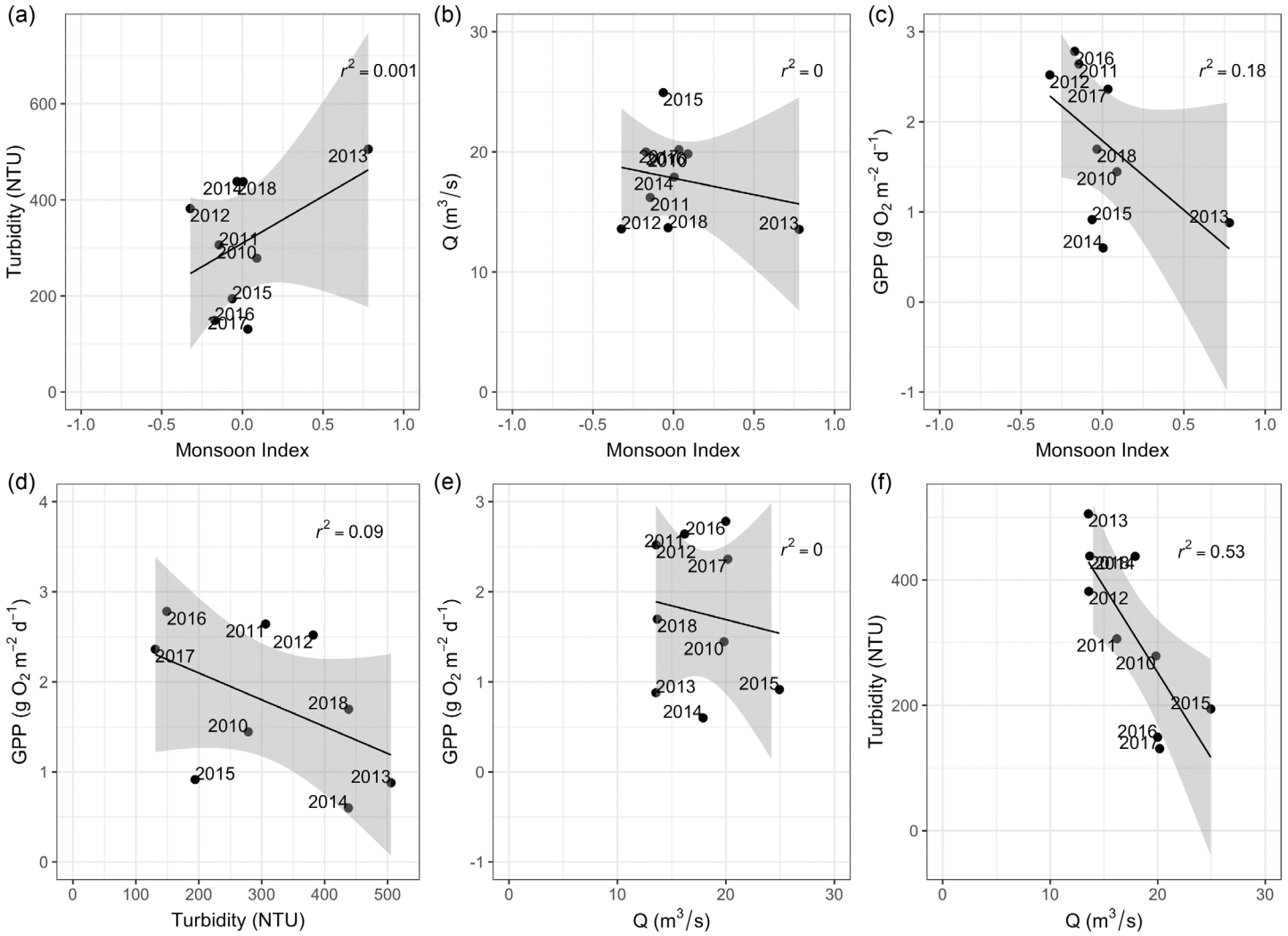

Fig. 6. During the summer monsoon period (July through September), relationships between mean turbidity and Monsoon Index ($r^2 = 0.001$), mean gross primary production (GPP) and Monsoon Index ($r^2 = 0.18$), and mean GPP and turbidity ($r^2 = 0.09$) were not evident. Note that GPP, turbidity, and *Q* are log transformed but show values on log scaled axes to ease interpretation.

higher-than-expected snowmelt discharge in 2017. Other climate-related disturbances, like the Las Conchas wildfire that burned within the contributing watershed in the summer 2011, not only had immediate impacts on water quality from rainfall runoff (Dahm et al. 2015; Reale et al. 2015) but had longer-term impacts on water clarity the following spring from snowmelt (Fig. 4), reducing our ability to parse the effect of ENSO on turbidity and hence GPP. Compounding factors including climate, disturbance, and antecedent conditions add to the multidimensionality of ecosystem response in space and time. Future research aimed at understanding these complex relationships will require the collection of multi-decade datasets.

The multilevel structure in this dataset (climate-disturbance-GPP) that we explored using HGAMs (Pedersen et al. 2019) also revealed that climate patterns explained the within-year effect of *Q* on daily GPP in the spring. The model structure including ONI as a random intercept and slope (i.e., intergroup variation) best captured these multilevel relationships and provides support for the hypothesis that ENSO affects GPP through *Q*, and to a lesser extent turbidity. Regardless of temporal scale, few studies have directly linked climate and stream metabolism signals and have instead relied on "space for time" approaches (Ulseth et al. 2018).

Summer monsoon controls on GPP

During the summer, our finding that turbidity covaried with GPP at the daily scale supported our hypothesis that annual averages during the monsoon period do not capture the influence of abrupt, short-lived disturbances on primary production. Instream conditions, including the frequency and duration of turbidity pulses within a year, which appear to influence the recovery trajectory of daily GPP following a disturbance (Summers 2019), do not additively explain annual

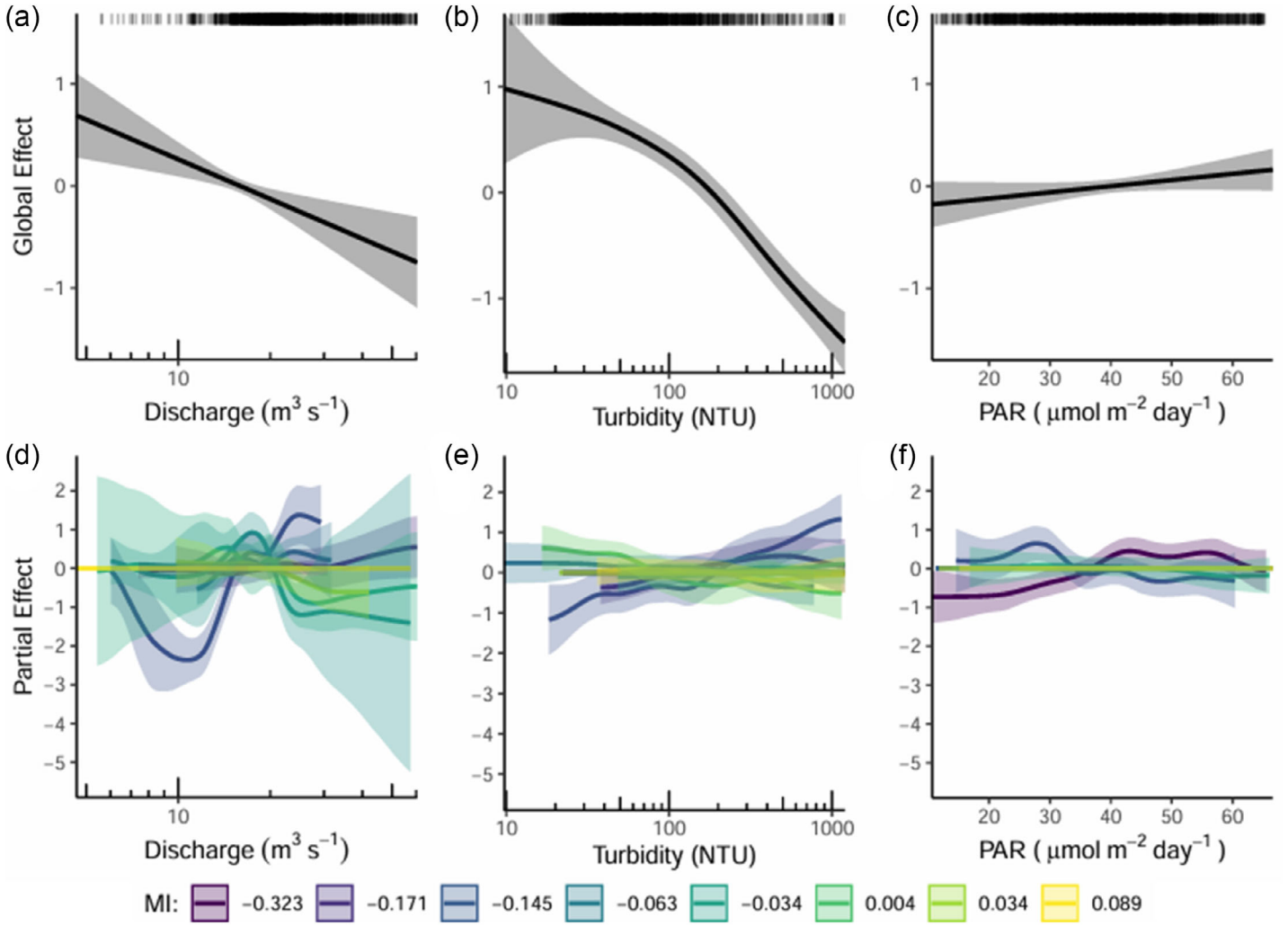

Fig. 7. Global smoother effects (**a**) discharge ($m^3\ s^{-1}$), (**b**) turbidity (NTU), and (**c**) photosynthetic active radiation ($\mu mol\ m^{-2}\ d^{-1}$) on daily GPP in summer. Group level variation in the effect of (**d**) discharge, (**e**) turbidity, and (**f**) PAR on daily GPP with Monsoon Index as the grouping variable. The effect on GPP varies from the global smoother when the response deviates from the zero *y*-axis. Legend shows MI groups. Discharge, turbidity, and GPP are log transformed. Upper ribbon in (**a**–**c**) represents data for predictors, and all plots have a 95% CI band around the smoothing trendline.

mean relationships between ecosystem processes and disturbance variables (Fig. 6d–f). Thus, while annual mean turbidity increased during the summer monsoon season compared to spring, the monsoon index we created to capture rainfall inputs within the immediate upstream catchment did not accurately predict summer mean GPP or turbidity levels at the annual time scale (Fig. 6a–c).

In contrast, at the daily scale, the global effect of turbidity (i.e., general trend in HGAMs) was a decrease in daily GPP. Although the global trend of *Q* also decreased daily GPP, the effect size was not as large (i.e., less negative) as turbidity (Fig. 7a, b), suggesting that turbidity was the predominant disturbance variable impacting GPP during summer months. While spring disturbances were linked to periods of elevated discharge detectable at the annual and daily scale, declines in GPP that occurred during the summer monsoon season coincided with increases in turbidity only at the daily scale. Additionally, we found annual mean turbidity to be inversely related to *Q* in summer (Fig. 6f). Our finding suggests that in arid land regions with highly erosive soils and sparse vegetation to prevent overland flow (Wilcox et al. 2003), relatively small quantities of water contribute high sediment loads to the mainstem of the river during the summer monsoon period, dramatically increasing turbidity with only small increases in discharge (Moore and Anderholm 2002). Thus, during the summer, sediment transport may be more important in controlling GPP than disturbance from flow due to increased light limitation as water clarity decreases (Fellows et al. 2009) as opposed to scouring from high discharge events.

Uncertainty in summer linkages between climate, disturbance, and ecosystem processes is likely influenced by

spatially isolated monsoon rainstorms and antecedent conditions that add complexity when observing at the larger time scale (i.e., annual averages). For example, soil characteristics, such as soil moisture, influence surface runoff and sediment mobilization during rainstorms (Seeger et al. 2004). Another potential influential factor contributing to data complexity includes interactions between climate phenomena; specifically, there is evidence that ENSO and the North American Monsoon are inversely correlated in the southwest United States (Gutzler 2000), although this relationship weakens outside the 1965–1992 period analyzed by Lo and Clark (2002), or that the timing of the monsoon season is delayed when snowpack is greater (Grantz et al. 2007). Uncertainty in parsing climate effects on disturbance variables and GPP could also stem from the need for longer-term data, even longer than the 9-yr data used in this study. Understanding linkages between monsoon climate patterns, disturbance, and carbon dynamics is needed because monsoon dynamics are predicted to change (i.e., onset, amount) with climate change (Hoell et al. 2015, Pascale et al. 2017), which will likely impact instream carbon dynamics.

Conclusions

Using 9 yr of continuous data we investigated the effect and certainty in global climate forcing on disturbance variables and gross primary production patterns in an aridland river. Climate affected watershed and ecosystem processes at annual and daily time scales, with regional to local conditions (i.e., wildfire disturbance and antecedent conditions) influencing the relationship between climate and gross primary production, and thus complicating inference. These findings highlight current knowledge gaps in the timing, magnitude, and duration of optimal organic carbon production as related to hydroclimatic variability (Bernhardt et al. 2018). This is a pressing area of research as changes in precipitation regimes (onset, intensity) and form (snowfall and rainfall types) are predicted, with likely impacts to instream carbon (Ulseth et al. 2018; Summers et al. 2020) and nutrient dynamics (Smits et al. 2019). Current questions include determining how much data are needed to detect climate effects on ecosystem processes, like stream metabolism, and creating and implementing time series modeling tools to parse fast and slow time-scale signals in environmental variables. We conclude that long-term datasets are essential to uncover emergent relationships between broad-scale climate patterns and ecosystem processes (Rudgers et al. 2018) and are necessary to better understand how hydroclimatic variability drives ecosystem processes in rivers across vast areas of Earth.

Author Contributions

Betsy M. Summers, Robert O. Hall Jr., and David J. Van Horn conceptualized this study. Betsy M. Summers, Robert O. Hall Jr., and David J. Van Horn contributed to the original writing of the paper. Betsy M. Summers led the data analysis. David J. Van Horn and Justin K. Reale contributed to the data collection. Eric Joseph and Mark C. Stone contributed to the methods. All authors participated in editing the manuscript and visualization.

Acknowledgments

Betsy M. Summers was supported by the Centers of Research Excellence in Science and Technology with funding from National Science Foundation award 1914778; Robert O. Hall Jr. was supported by the Modelscape project with funding from National Science Foundation award 2019528; the U.S. Army Corps of Engineers' (USACE) Middle Rio Grande Endangered Species Collaborative Program provided funding to Betsy M. Summers and Justin K. Reale; Mark C. Stone was supported by the Center for Water and Environment with funding from National Science Foundation award 1345169. The USACE Upper Rio Grande Water Operations Model supported continuous water quality data collection through internal funding to Justin K. Reale and Cooperative Agreement W912HZ-14-2-0014 to David J. Van Horn. We thank the two anonymous reviewers for helping improve the presentation of this paper. Any opinion, finding, and conclusion or recommendation expressed in this material are those of the authors and do not necessarily reflect the views of the U.S. Army Corps of Engineers or the United States.

Conflicts of Interest

None declared.

Data Availability Statement

Daily water quality data are archived and accessible through the Environmental Data Initiative (https://doi.org/10.6073/pasta/6aa506029798d7c0bbbce5b9d83eaede).

References

Acuña, V., I. Muñoz, A. Giorgi, M. Omella, F. Sabater, and S. Sabater. 2005. "Drought and Postdrought Recovery Cycles in an Intermittent Mediterranean Stream: Structural and Functional Aspects." *Journal of the North American Benthological Society* 24: 919–933. https://doi.org/10.1899/04-078.1.

Akaike, H. 1979. "A Bayesian Extension of the Minimum AIC Procedure of Autoregressive Model Fitting." *Biometrika* 66: 237–242. https://doi.org/10.1093/biomet/66.2.237.

Appling, A. P., R. O. Hall, C. B. Yackulic, and M. Arroita. 2018. "Overcoming Equifinality: Leveraging Long Time Series for Stream Metabolism Estimation." *Journal of Geophysical Research – Biogeosciences* 123: 624–645. https://doi.org/10.1002/2017JG004140.

Arroita, M., A. Elosegi, and R. O. Hall. 2019. "Twenty Years of Daily Metabolism Show Riverine Recovery Following

Sewage Abatement." *Limnology and Oceanography* 64: S77–S92. https://doi.org/10.1002/lno.11053.

Atkinson, B. L., M. R. Grace, B. T. Hart, and K. E. N. Vanderkruk. 2008. "Sediment Instability Affects the Rate and Location of Primary Production and Respiration in a Sand-Bed Stream." *J. North Am. Benthol. Soc.* 27: 581–592. https://doi.org/10.1899/07-143.1.

Beaulieu, J. J., C. Arango, D. A. Balz, and W. D. Shuster. 2013. "Continuous Monitoring Reveals Multiple Controls on Ecosystem Metabolism in a Suburban Stream." *Freshwater Biology* 58: 918–937. https://doi.org/10.1111/fwb.12097.

Bernhardt, E. S., P. Savoy, M. J. Vlah, et al. 2022. "Light and Flow Regimes Regulate the Metabolism of Rivers." *Proceedings of the National Academy of Sciences* 119, no. 8. https://doi.org/10.1073/pnas.2121976119.

Bernhardt, E. S., J. B. Heffernan, N. B. Grimm, et al. 2018. "The Metabolic Regimes of Flowing Waters." *Limnology and Oceanography* 63: S99–S118. https://doi.org/10.1002/lno.10726.

Breheny P., W. Burchett. 2017. "Visualization of Regression Models Using visreg." *The R Journal* 9(2): 56–71. https://doi.org/10.32614/CRAN.package.visreg

Canadell, M. B., L. Gómez-Gener, A. J. Ulseth, M. Clémençon, S. N. Lane, and T. J. Battin. 2021. "Regimes of Primary Production and Their Drivers in Alpine Streams." *Freshwater Biology* 66: 1449–1463. https://doi.org/10.1111/fwb.13730.

Clark, C., G. A. Nnaji, and W. Huang. 2014. "Effects of El-Niño and La-Niña Sea Surface Temperature Anomalies on Annual Precipitations and Streamflow Discharges in Southeastern United States." *Journal of Coastal Research* 68: 113–120. https://doi.org/10.2112/SI68-015.1.

Dahm, C. N., R. I. Candelaria-Ley, C. S. Reale, J. K. Reale, and D. J. Van Horn. 2015. "Extreme Water Quality Degradation Following a Catastrophic Forest Fire." *Freshwater Biology* 60: 2584–2599. https://doi.org/10.1111/fwb.12548.

Davis, C. M., C. Bahner, D. Eidson, and S. Gibson. 2014. "Understanding Reservoir Sedimentation along the Rio Grande: A Case Study from Cochiti Dam." In World Environmental and Water Resources Congress, 2347–2357.

Dettinger, M. D., and H. F. Diaz. 2000. "Global Characteristics of Stream Flow Seasonality and Variability." *Journal of Hydrometeorology* 1: 289–310. https://doi.org/10.1175/1525-7541(2000)001<0289:GCOSFS>2.0.CO;2.

Dettinger, M. D., F. M. Ralph, T. Das, P. J. Neiman, and D. R. Cayan. 2011. "Atmospheric Rivers, Floods and the Water Resources of California." *Water* 3: 445–478. https://doi.org/10.3390/w3020445.

Dodds, W. K., S. A. Higgs, M. J. Spangler, et al. 2018. "Spatial Heterogeneity and Controls of Ecosystem Metabolism in a Great Plains River Network." *Hydrobiological Journal* 813: 85–102. https://doi.org/10.1007/s10750-018-3516-0.

Duan, S., P. Ullrich, and W. R. Boos. 2024. "Meteorological Drivers of North American Monsoon Extreme Precipitation Events." *Journal of Geophysical Research-Atmospheres* 129: e2023JD040535. https://doi.org/10.1029/2023JD040535.

Edmund, H., K. Bell, and A. Butler. 2025. Access Data from the Oregon State Prism Climate Project.

Fellows, C. S., S. E. Bunn, F. Sheldon, and N. J. Beard. 2009. "Benthic Metabolism in Two Turbid Dryland Rivers." *Freshwater Biology* 54: 236–253. https://doi.org/10.1111/j.1365-2427.2008.02104.x.

Gelman, A., X.-L. Meng, and H. Stern. 1996. "Posterior Predictive Assessment of Model Fitness Via Realized Discrepancies." *Statistica Sinica* 6: 733–807.

Gochis, D. J., L. Brito-Castillo, and W. J. Shuttleworth. 2006. "Hydroclimatology of the North American Monsoon Region in Northwest Mexico." *Journal of Hydrology* 316: 53–70. https://doi.org/10.1016/j.jhydrol.2005.04.021.

Grantz, K., B. Rajagopalan, M. Clark, and E. Zagona. 2007. "Seasonal Shifts in the North American Monsoon." *Journal of Climate* 20: 1923–1935. https://doi.org/10.1175/JCLI4091.1.

Gutzler, D. S. 2000. "Covariability of Spring Snowpack and Summer Rainfall across the Southwest United States." *Journal of Climate* 13: 4018–4027. https://doi.org/10.1175/1520-0442(2000)013<4018:COSSAS>2.0.CO;2.

Gutzler, D. S. 2004. "An Index of Interannual Precipitation Variability in the Core of the North American Monsoon Region." *Journal of Climate* 17: 4473–4480. https://doi.org/10.1175/3226.1.

Hoell, A., C. Funk, M. Barlow, and S. Shukla. 2015. "Recent and Possible Future Variations in the North American Monsoon." In The Monsoons and Climate Change, edited by L. de Carvalho and C. Jones. Springer Climate.

Hosen, J. D., K. S. Aho, A. P. Appling, et al. 2019. "Enhancement of Primary Production During Drought in a Temperate Watershed Is Greater in Larger Rivers Than Headwater Streams." *Limnology and Oceanography* 64: 1458–1472. https://doi.org/10.1002/lno.11127.

Jähne, B., K. O. Münnich, R. Bösinger, A. Dutzi, W. Huber, and Libner. 1987. "On the Parameters Influencing Air-Water Gas Exchange." *Journal of Geophysical Research* 92: 1937–1949. https://doi.org/10.1029/JC092iC02p01937.

Julian, J. P., M. W. Doyle, and E. H. Stanley. 2008. "Empirical Modeling of Light Availability in Rivers." *Journal of Geophysical Research – Biogeosciences* 113: G3. https://doi.org/10.1029/2007JG000601.

Keener, V. W., G. W. Feyereisen, U. Lall, J. W. Jones, D. D. Bosch, and R. Lowrance. 2010. "El-Niño/Southern Oscillation (ENSO) Influences on Monthly NO3 Load and Concentration, Stream Flow and Precipitation in the Little River Watershed, Tifton, Georgia (GA)." *Journal of Hydrology* 381: 352–363. https://doi.org/10.1016/j.jhydrol.2009.12.008.

Kirk, L., R. T. Hensley, P. Savoy, J. B. Heffernan, and M. J. Cohen. 2021. "Estimating Benthic Light Regimes Improves Predictions of Primary Production and Constrains Light-

Use Efficiency in Streams and Rivers." *Ecosystem* 24: 825–839. https://doi.org/10.1007/s10021-020-00552-1.

Leopold, L. B., and T. Maddock. 1953. The Hydraulic Geometry of Stream Channels and Some Physiographic Implications. Vol. 252, 57. U.S. Geological Survey Professional Paper.

Lo, F., and M. P. Clark. 2002. "Relationships Between Spring Snow Mass and Summer Precipitation in the Southwestern United States Associated with the North American Monsoon System." *Journal of Climate* 15: 1378–1385. https://doi.org/10.1175/1520-0442(2002)015<1378:rbssma>2.0.co;2.

Lusk, J. D. (2006–2008) 2012. Rio Grande Silvery Minnow Health study Introduction With Results of Water Quality Parameters Measured and Derivation of Gross Primary Productivity and Ecosystem Respiration in the Middle Rio Grande, New Mexico, 189. Albuquerque, New Mexico: U.S. Fish and Wildlife Service, New Mexico Ecological Services.

Marzolf, N. S., M. J. Vlah, H. E. Lowman, W. M. Slaughter, and E. S. Bernhardt. 2024. "Phenology of Gross Primary Productivity in Rivers Displays High Variability Within Years but Stability across Years." *Limnology and Oceanography* 9: 524–531. https://doi.org/10.1002/lol2.10407.

Massong, T., P. Makar, and T. Bauer. 2010. "Planform Evolution Model for the Middle Rio Grande, NM." In Proceedings of the 2nd Joint Federal Interagency Conference, Las Vegas, NV.

Massong, T., P. Tashjian, and P. Makar. 2006. "Recent Channel Incision and Floodplain Evolution Within in the Middle Rio Grande, NM." In Proceedings of the Eighth Federal Interagency Sedimentation Conference, 216–224.

McNamara, J. P., D. Chandler, M. Seyfried, and S. Achet. 2005. "Soil Moisture States, Lateral Flow, and Streamflow Generation in a Semi-Arid, Snowmelt-Driven Catchment." *Hydrological Processes* 19: 4023–4038. https://doi.org/10.1002/hyp.5869.

Meek, D. W., J. L. Hatfield, T. A. Howell, S. B. Idso, and R. J. Reginato. 1984. "A Generalized Relationship Between Photosynthetically Active Radiation and Solar Radiation." *Agronomy Journal* 76: 939–945. https://doi.org/10.2134/agronj1984.00021962007600060018x.

Molles, M. C., Jr., and C. N. Dahm. 1990. "A Perspective on El Nino and La Nina: Global Implications for Stream Ecology." *J. North Am. Benthol. Soc.* 9: 68–76. https://doi.org/10.2307/1467935

Moore, S. J., and S. K. Anderholm. 2002. "Spatial and Temporal Variations in Streamflow, Dissolved Solids, Nutrients, and Suspended Sediment in the Rio Grande Valley Study Unit, Colorado, New Mexico, and Texas, 1993–95." In Water-Resources Investigations Report. Denver, CO: U.S. Geological Survey.

Morera, S. B., T. Condom, A. Crave, P. Steer, and J. L. Guyot. 2017. "The Impact of Extreme El Niño Events on Modern Sediment Transport along the Western Peruvian Andes (1968–2012)." *Scientific Reports* 7: 11947. http://doi.org/10.1038/s41598-017-12220-x.

Nordin, C. F. J., and J. P. Beverage. 1965. Sediment Transport in the Rio Grande New Mexico. U.S. Government Printing Office.

O'Connor, B. L., J. W. Harvey, and L. E. McPhillips. 2012. "Thresholds of Flow-Induced Bed Disturbances and Their Effects on Stream Metabolism in an Agricultural River." *Water Resources Research* 48: W08504. https://doi.org/10.1029/2011WR011488.

Odum, H. T. 1956. "Primary Production in Flowing Waters." *Limnology and Oceanography* 1: 102–117. https://doi.org/10.4319/lo.1956.1.2.0102.

Ortiz, R. M. 2004. A River in Transition: Geomorphic and Bed Sediment Response to Cochiti Dam on the Middle Rio Grande, Bernalillo to Albuquerque, New Mexico. University of New Mexico.

Pascale, S., W. R. Boos, S. Bordoni, et al. 2017. "Weakening of the North American Monsoon With Global Warming." *Nature Climate Change* 7: 806–812. https://doi.org/10.1038/nclimate3412.

Pedersen, E. J., D. L. Miller, G. L. Simpson, and N. Ross. 2019. "Hierarchical Generalized Additive Models in Ecology: An Introduction with mgcv." *PeerJ* 7: e6876. https://doi.org/10.7717/peerj.6876.

Pellerin, B. A., J. F. Saraceno, J. B. Shanley, et al. 2012. "Taking the Pulse of Snowmelt: In Situ Sensors Reveal Seasonal, Event and Diurnal Patterns of Nitrate and Dissolved Organic Matter Variability in an Upland Forest Stream." *Biogeochemistry* 108: 183–198. https://doi.org/10.1007/s10533-011-9589-8.

Reale, J. K., D. J. Van Horn, K. E. Condon, and C. N. Dahm. 2015. "The Effects of Catastrophic Wildfire on Water Quality along a River Continuum." *Freshwater Science* 34: 1426–1442. https://doi.org/10.1086/684001.

Regier, P. J., R. González-Pinzón, D. J. Van Horn, J. K. Reale, J. Nichols, and A. Khandewal. 2020. "Water Quality Impacts of Urban and Non-Urban Arid-Land Runoff on the Rio Grande." *Science of the Total Environment* 729: 138443. https://doi.org/10.1016/j.scitotenv.2020.138443.

Ropelewski, C. F., and M. S. Halpert. 1996. "Quantifying Southern Oscillation-Precipitation Relationships." *Journal of Climate* 9: 1043–1059. https://doi.org/10.1175/1520-0442(1996)009<1043:QSOPR>2.0.CO;2.

Rudgers, J. A., Y. A. Chung, G. E. Maurer, et al. 2018. "Climate Sensitivity Functions and Net Primary Production: A Framework for Incorporating Climate Mean and Variability." *The Ecologist* 99: 576–582. https://doi.org/10.1002/ecy.2136.

Sagarika, S., A. Kalra, and S. Ahmad. 2015. "Interconnections Between Oceanic–Atmospheric Indices and Variability in the US Streamflow." *Journal of Hydrology* 525: 724–736. https://doi.org/10.1016/j.jhydrol.2015.04.020.

Savoy, P., A. P. Appling, J. B. Heffernan, et al. 2019. "Metabolic Rhythms in Flowing Waters: An Approach for Classifying River Productivity Regimes." *Limnology and Oceanography* 64: 1835–1851. https://doi.org/10.1002/lno.11154.

Sebestyen, S. D., E. W. Boyer, J. B. Shanley, et al. 2008. "Sources, Transformations, and Hydrological Processes that Control Stream Nitrate and Dissolved Organic Matter Concentrations during Snowmelt in an Upland Forest." *Water Resources Research* 44: W12410. https://doi.org/10.1029/2008WR006983.

Seeger, M., M. P. Errea, S. Begueria, J. Arnáez, C. Martı, and J. M. Garcıa-Ruiz. 2004. "Catchment Soil Moisture and Rainfall Characteristics as Determinant Factors for Discharge/Suspended Sediment Hysteretic Loops in a Small Headwater Catchment in the Spanish Pyrenees." *Journal of Hydrology* 288: 299–311. https://doi.org/10.1016/j.jhydrol.2003.10.012.

Simpson, G. L., and H. Singmann. 2021. Gratia: Graceful 'ggplot'-Based Graphics and Other Functions for GAMs Fitted Using 'mgcv' (0.6. 0). CRAN (Comprehensive R Archive Network).

Smits, A. P., C. M. Ruffing, T. V. Royer, et al. 2019. "Detecting Signals of Large-Scale Climate Phenomena in Discharge and Nutrient Loads in the Mississippi-Atchafalaya River Basin." *Geophysical Research Letters* 46: 3791–3801. https://doi.org/10.1029/2018GL081166.

Stone, R. C., G. L. Hammer, and T. Marcussen. 1996. "Prediction of Global Rainfall Probabilities Using Phases of the Southern Oscillation Index." *Nature* 384: 252–255. https://doi.org/10.1038/384252a0.

Summers, B. M. 2019. "Multi-Year Water Quality Data Reveal Highly Variable Timing and Magnitude of Metabolism and Physicochemical Drivers in an Aridland River Network." Doctoral dissertation, The University of New Mexico.

Summers, B. M., D. J. Van Horn, R. González-Pinzón, et al. 2020. "Long-Term Data Reveal Highly-Variable Metabolism and Transitions in Trophic Status in a Montane Stream." *Freshwater Science* 39: 241–255. https://doi.org/10.1086/708659.

Swanson, B. J., G. A. Meyer, and J. E. Coonrod. 2011. "Historical Channel Narrowing along the Rio Grande Near Albuquerque, New Mexico in Response to Peak Discharge Reductions and Engineering: Magnitude and Uncertainty of Change from Air Photo Measurements." *Earth Surface Processes* 36: 885–900. https://doi.org/10.1002/esp.2119.

Uehlinger, U., and M. W. Naegeli. 1998. "Ecosystem Metabolism, Disturbance, and Stability in a Prealpine Gravel Bed River." *J. North Am. Benthol. Soc.* 17: 165–178. https://doi.org/10.2307/1467960.

Ulseth, A. J., E. Bertuzzo, G. A. Singer, J. Schelker, and T. J. Battin. 2018. "Climate-Induced Changes in Spring Snowmelt Impact Ecosystem Metabolism and Carbon Fluxes in an Alpine Stream Network." *Ecosystem* 21: 373–390. https://doi.org/10.1007/s10021-017-0155-7.

Ulseth, A. J., R. O. Hall Jr., M. B. Canadell, H. L. Madinger, A. Niayifar, and T. J. Battin. 2019. "Distinct Air-Water Gas Exchange Regimes in Low- and High-Energy Streams." *Nature Geoscience* 12: 259–263. https://doi.org/10.1038/s41561-019-0324-8.

Van Horn, D. J., and B. Summers. 2025. "Middle Rio Grande New Mexico, Bernalillo 550 Bridge, Water Quality Daily Means 2010-2018 Ver 1." Environmental Data Initiative. Accessed July 7, 2025. https://doi.org/10.6073/pasta/6aa506029798d7c0bbbce5b9d83eaede.

Wagner, R. J., R. A. Kimbrough, and G. L. Turney. 2007. "Quality-Assurance Plan for Water-Quality Activities in the U.S. Geological Survey Washington Water Science Center." U.S. Geological Survey Open-File Report 2007-1307 https://doi.org/10.1038/nnano.2007.401.

Wanders, N., and Y. Wada. 2015. "Decadal Predictability of River Discharge with Climate Oscillations over the 20th and Early 21st Century." *Geophysical Research Letters* 42: 10–689. https://doi.org/10.1002/2015GL066929.

Wilcox, B. P., D. D. Breshears, and C. D. Allen. 2003. "Ecohydrology of a Resource-Conserving Semiarid Woodland: Effects of Scale and Disturbance." *Ecological Monographs* 73: 223–239. https://doi.org/10.1890/0012-9615(2003)073[0223:EOARSW]2.0.CO;2.

Wood, S. N. 2017. Generalized Additive Models: An Introduction With R. 2nd ed. Chapman and Hall/CRC.

Wood, S. N. 2011. "Fast Stable Restricted Maximum Likelihood and Marginal Likelihood Estimation of Semi-parametric Generalized Linear Models." *Journal of the Royal Statistical Society, Series B (Statistical Methodology)* 73: 3–36. https://doi.org/10.1111/j.1467-9868.2010.00749.x.

Young, R. G., and A. D. Huryn. 1996. "Interannual Variation in Discharge Controls Ecosystem Metabolism along a Grassland River Continuum." *Canadian Journal of Fisheries and Aquatic Sciences* 53: 2199–2211. https://doi.org/10.1139/f96-186.

Zeileis, A., and G. Grothendieck. 2005. "zoo: S3 Infrastructure for Regular and Irregular Time Series." *Journal of Statistical Software* 14: 1–27. https://doi.org/10.18637/jss.v014.

Supporting Information

Additional Supporting Information may be found in the online version of this article.

Submitted 12 February 2024
Revised 23 January 2025
Accepted 30 July 2025